

Photoionization of the Ne-like Si^{4+} ion in ground and metastable states in the 110–184-eV photon energy range

J.-M. Bizau,^{1,*} J.-P. Mosnier,² E. T. Kennedy,² D. Cubaynes,¹ F. J. Wuilleumier,¹ C. Blancard,³ J.-P. Champeaux,^{3,†} and F. Folkmann⁴

¹Laboratoire d'Interaction des rayons X avec la Matière, Bât. 350, Université Paris-Sud, F-91405 Orsay Cedex, France

²National Centre for Plasma Science and Technology, School of Physical Sciences, Dublin City University, Glasnevin, Dublin 9, Ireland

³CEA, DAM, DIF, F-91297 Arpajon, France

⁴Department of Physics and Astronomy, University of Aarhus, DK-8000 Aarhus C, Denmark

(Received 12 January 2009; published 16 March 2009)

We present measurements of the absolute photoionization cross section of the neonlike Si^{4+} ion over the 110–184 eV photon energy range. The measurements were performed using two independent merged-beam setups at the super-ACO and ASTRID synchrotron-radiation facilities, respectively. Signals produced in the photoionization of the $2p$ subshell of the Si^{4+} ion both from the $2p^6\ ^1S_0$ ground state and the $2p^53s\ ^3P_{0,2}$ metastable levels were observed. Calculations of the $2p$ photoionization cross sections were carried out using a multi-configuration Dirac-Fock code. They give results in good agreement with the measured spectra. Comparison with other available theoretical results is also presented.

DOI: 10.1103/PhysRevA.79.033407

PACS number(s): 32.80.Fb, 32.80.Zb

I. INTRODUCTION

The understanding and modeling of matter in the plasma state, whether natural or artificial, requires the knowledge of many atomic data. For example, the absolute photoionization cross sections of neutrals and ions and the energies and oscillator strengths of discrete transitions are needed for the determination of plasma opacities and plasma diagnostics, respectively. Large international collaborations motivated particularly by astrophysical needs, such as the Opacity Project (OP) [1] or the Iron Project [2], have endeavored to calculate these data for an extended range of ionic species, using the R -matrix model to describe electron correlation effects. Atomic databases [3] provide key data for a wide range of users and require experimental data providing, in particular, absolute cross sections to facilitate benchmarking of the various theoretical approaches.

To obtain experimental values to test the validity of the theoretical predictions requires the production of high-density ionic targets at the site of high-flux photon sources. Plasma sources can be used for both purposes and a range of relative photoabsorption cross sections were obtained over many years using the dual laser plasma (DLP) technique, see for example Refs. [4–6]. More recently with the advent of high-photon fluxes delivered by insertion devices at third generation synchrotron-radiation (SR) facilities, merged-beam setups have been developed, allowing the determination of the photoionization cross sections for singly and multiply ionized species on an *absolute* scale [7–10]. The latest development of short-wavelength free-electron laser (FEL) sources is opening up new regimes in terms of the interaction of ionizing radiation with dilute atomic and molecular species [11–13].

Neonlike ions, because of their closed shells in the ground state (configuration: $1s^22s^22p^6$) and significant cosmic abundance have been extensively studied using a variety of theoretical approaches [14–21]. In a study of the low end of the neon isoelectronic series, using a combination of relativistic random-phase approximation (RRPA) together with relativistic multichannel quantum-defect theory (RMQDT), it was shown that even for the early series members Ne, Na^+ , and Mg^{2+} the photoionization behavior between the $^2P_{3/2}$ and $^2P_{1/2}$ limits varies quite dramatically [22]. Near threshold photoionization resonances directly affect the inverse process of dielectronic recombination for low-energy electrons and hence can alter the total recombination rates significantly for a diverse range of astrophysical and laboratory plasmas. The important role of inner-shell resonances has been emphasized in a combined experimental and theoretical study of neonlike ions based on DLP photoabsorption data and RRPA calculations, respectively [5]. For Si^{4+} , the calculated threshold cross section was more than 1 order of magnitude below that anticipated from an isoelectronic interpolation up to $Z=100$. This calculated anomalous behavior in the near-threshold photoionization cross section was explained as due to the inner-shell $2s \rightarrow 3p$ resonance lying just below the ionization threshold for Si^{4+} . The RRPA calculations were complemented by a series of DLP experiments for the early members of the sequence up to Si^{4+} , which showed clearly that the $2s \rightarrow 3p$ resonance for Si^{4+} lies at 165.4 eV, below the measured $2s^22p^5\ ^2P_{3/2, 1/2}$ thresholds at 166.7 and 167.2 eV [5]. The plasma experiments nevertheless indicated an asymmetric Fano profile for the $2s \rightarrow 3p$ resonance, which was attributed to plasma microfields lowering the ionization limit, resulting in a case of forced autoionization.

Motivated, in particular, by the previous work on Si^{4+} , we present here the first results of an experimental study of the *absolute* photoionization cross section of the Si^{4+} ion in the $2p$ threshold photon region, using the merged-beam photoion setups of super-ACO in Orsay (France) and ASTRID in Aarhus (Denmark), respectively. The plasma environment ef-

*Corresponding author. jean-marc.bizau@u-psud.fr

†Present address: IRSAMC LCAR, UMR 5589—Université Paul Sabatier, 118 Route de Narbonne, 31062 Toulouse CEDEX, France

TABLE I. Main characteristics differing between the super-ACO and ASTRID experiments.

	Super-ACO	ASTRID
Acceleration voltage	7 kV	6 kV
Magnetic filter	Wien	Dipole
Retardation system	After the filter	Before the filter
Energy of the ions in the interaction region	16 keV	4.8 keV
Length of the interaction	20 cm	50 cm
Current of ions in the interaction region	120 nA	25 nA
Charge analyzer	Electrostatic	Magnetic
Energy resolution $\Delta h\nu/h\nu$	0.5%	1.5%

fects just mentioned are not present in synchrotron merged-beam experiments because of the very low density of ions achieved in the interaction region, compared to plasma experiments. Multiconfiguration Dirac-Fock (MCDHF) calculations have also been performed to identify various features observed in the spectra. The results are compared with all available theoretical data and the above mentioned DLP photoabsorption data.

II. EXPERIMENTAL DETAILS AND RESULTS

Detailed descriptions of the experimental super-ACO and ASTRID setups and procedures used in our merged-beam measurements can be found in Refs. [23,24], respectively. Both setups are quite similar, with the main differences being that the super-ACO setup is a more compact apparatus, optimized for an electron cyclotron resonance ion source (ECRIS). The ASTRID setup, originally designed for use with a singly-charged ion source, is better suited to the determination of accurate absolute photoionization cross sections while the super-ACO facility provides higher ion currents allowing the use of better spectral resolving power. The principal characteristics of the two setups are summarized in Table I.

The experimental details relevant to the present study are now described briefly. The silicon ions were produced, from silane, in a permanent magnet ECRIS driven by a 20 W, 10 GHz microwave power supply. The same source was used for both experiments. After extraction, the Si^{4+} ions were selected using a magnetic filter, and merged with the synchrotron-radiation beam. Following the interaction of the two beams in a spatially well defined interaction region, the incident ions were separated from the ions which had gained one positive charge in the interaction (the so-called photoions) using a charge-state analyzer. The parent ions were collected in a Faraday cup, and the photoions were counted with an electron multiplier detector. The characteristics of the super-ACO SU6 and ASTRID Miyake SR beam lines are also quite similar. Both use an undulator as the photon source which, after monochromatization, delivers photons in the 20–185 eV energy range. Flux is also of the same order for both sources, typically some 10^{12} photons/s in 0.1% bandwidth. In both setups, the photon energy was calibrated using

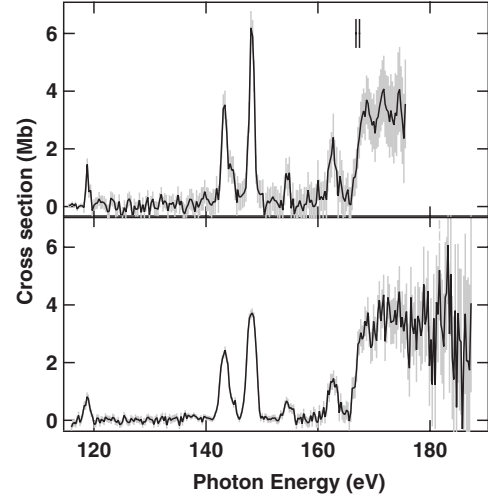


FIG. 1. Photoionization cross section of Si^{4+} ion measured between 115 and 185 eV photon energy at super-ACO (upper panel) and ASTRID (lower panel). Error bars (in light gray) indicate the statistical uncertainties. The two black vertical bars give the position of the previously measured ionization thresholds [5].

a gas cell and the $3d \rightarrow 5p$ lines of Kr [3] and $2p_{1/2} \rightarrow t_{2g}$ line of SF_6 [25].

The measured photoionization cross sections, as obtained from the variations of the Si^{5+} photoion counting rate recorded by the detectors as a function of photon energy, are presented in Fig. 1. The upper panel shows the super-ACO data, with the light gray indicating the statistical error bars. The lower panel shows the corresponding data obtained at ASTRID.

Although both setups have the capability to determine absolute photoionization cross sections, due to limited beam time it was only possible to measure relative cross sections at super-ACO. These were placed later on an absolute scale by normalization to the ASTRID absolute measurements through a comparison of the spectra between 165 and 175 eV. The total uncertainty in the cross-section values is determined by the statistical fluctuations plus systematic contributions estimated to be of the order of 10%–15% [24]. Above about 180 eV the statistical fluctuations increase rapidly in the data due to the fall off in the photon flux.

Taking into account the difference in spectral resolution (see Table I and Fig. 1) between the two measurements, we note the good agreement between the two sets of data. The known positions of the $\text{Si}^{5+} 2P_{3/2,1/2}$ ionization thresholds [5] are indicated on Fig. 1 by the two black vertical bars. Several strong lines are observed at lower photon energies. They are the signature that Si^{4+} ions in the $2p^5 3s^3 P_{J=0,2}$ metastable levels are contributing to the photoionization spectra, despite their high excitation energy of around 104 eV [3]. These excited ions are produced in the ECRIS and have a lifetime long enough (8.9 ms for the $J=2$ level and 1.4 s for the $J=0$ level [26]) to remain appreciably populated in the interaction chamber. The ionic target beam was therefore a mixture of ions in the $2s^2 2p^6 1S_0$ ground and $2s^2 2p^5 3p^3 P_{0,2}$ excited states, respectively. We have also checked there was no contamination of the target due N^{2+} ions by looking for N^{3+} photoion signals while keeping the same ECRIS condi-

tions used during the recording of the Si⁴⁺ spectrum [27]. Even when increasing the photon flux to its maximum value, no N³⁺ signal was detected, showing that a contribution of N²⁺ ion was negligible.

III. CALCULATIONS

Ab initio calculations of the photoionization of Si⁴⁺ were performed to interpret the experimental spectra, using the MCDF code developed by Bruneau [28]. For photoexcitation, 281 levels constructed from the configurations: $2p^53s$, $2p^43s ns$ and $2p^43s nd$, with $n=3-6$ were included. Photoexcitation cross sections from the levels of the $2p^53s$ configuration were computed assuming Lorentzian profiles with 10 meV full widths at half maximum (FWHM) for the shape of all excitation lines present in the experimentally investigated photon energy range. The theoretical results were then convolved with a Gaussian function with a constant value of 1 eV FWHM to account for the finite experimental resolution.

For the direct photoionization cross section for Si⁴⁺ ion in the ground state, only the final Si⁵⁺ $2p^5$ configuration was considered and the cross section was calculated at a regular interval of 0.5 eV on the photon energy scale. The length form of the electric-dipole operator was used for all the present cross-section calculations. The total photoionization cross section was obtained as a sum of the ground- and excited-states cross sections, neglecting possible interference terms.

IV. ANALYSIS AND COMPARISON WITH THEORY

The comparison of our theoretical results with the experimental spectrum recorded at super-ACO is shown in Fig. 2. The upper panel shows the super-ACO data of Fig. 1 without the statistical error bars, the second panel shows the calculated theoretical synthetic spectrum and the lower two panels show the MCDF results (3P_2 and 3P_0 , respectively) before summing and convolving for the experimental resolution. To construct the theoretical synthetic spectrum σ_{th} , we used a weighted sum of individual total photoionization MCDF calculated cross sections $\sigma^{(2S+1)L_j}$ following the equation,

$$\sigma_{th} = 0.89\sigma(^1S_0) + 0.11\{5/6\sigma(^3P_2) + 1/6\sigma(^3P_0)\}.$$

The cross section for the 1S_0 , multiplied by the relative population (89%) of ions in the ground state, is shown as the dashed curve on the second panel of Fig. 2. The relative population of ions in the two metastable levels was estimated at 11% by comparing the experimental and calculated spectra for the area under the line at 148.2 eV. Subsequently, the individual contributions of the metastable levels were calculated, assuming that their populations were in the ratio of their statistical weights. This procedure brings the super-ACO and the synthetic MCDF spectra into good agreement, allowing us to suggest assignments for the observed lines. The proposed identifications are given in Table II, together with the calculated and measured positions and the oscillator strengths of the lines observed below the ionization thresholds. All arise from resonant photoionization of the $3s$ sub-

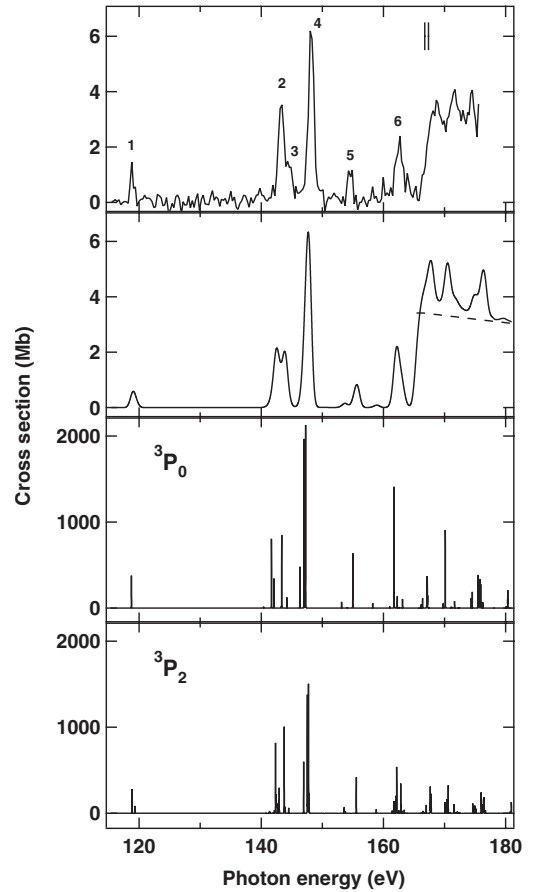
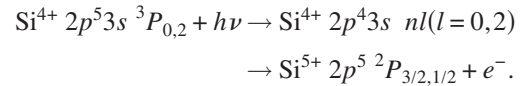


FIG. 2. Comparison of the super-ACO experimental spectrum (top panel) with the theoretical synthetic MCDF spectrum (second panel). The lower two panels show the MCDF results (resonance structures only) before convolution for the experimental spectral resolution. The dashed curve on the second panel represents the MCDF cross section for the 1S_0 ground state, multiplied by 0.89 (see text).

shell in the metastable ions following the processes:



From the experimental values, the oscillator strengths were extracted from the areas under the lines following the equation [29]:

$$f = 9.11 \times 10^{-3} \int_{h\nu_1}^{h\nu_2} \sigma(h\nu) dh\nu,$$

and subsequently dividing by 0.11 to correct for the population of the metastable levels. Due to the limited experimental resolution, they are the sum of several transitions from the two initial levels. To compare the theoretical and the experimental values, it is necessary to calculate for each line the sum of the corresponding theoretical oscillator strengths weighted by the statistical weight of the initial level.

Figure 1 also provides evidence for resonant structures just above the $2p$ photoionization limits. These can also be accounted for in terms of the MCDF calculations as shown

TABLE II. Comparison of the energies and oscillator strengths of the observed lines. The assignments given in the last column correspond to the photoionization process $\text{Si}^{4+}2p^53s^3P_{0,2}+h\nu \rightarrow \text{Si}^{4+}2p^43s\ n l\ 2^{S+1}L_J$.

Line ^a	Energy ^b (eV)			Oscillator strength ^b			Assignment
	SACO	ASTRID	MCDF	SACO	ASTRID	MCDF	
1	118.81 (7)	118.80 (8)	118.77	0.058(11)	0.064(8)	0.054	$^3P_0 \rightarrow 3s\ ^3P_1$
			118.88			0.040	$^3P_2 \rightarrow 3s\ ^3P_2$
			119.38			0.013	$^3P_2 \rightarrow 3s\ ^3P_1$
2	143.25 (7)	143.36 (5)	141.69	0.312(38)	0.357(11)	0.123	$^3P_0 \rightarrow 3d\ ^3D_1$
			142.09			0.054	$^3P_0 \rightarrow 3d\ ^3P_1$
			142.35			0.119	$^3P_2 \rightarrow 3d\ ^3D_3$
			142.38			0.033	$^3P_2 \rightarrow 3d\ ^3D_2$
			142.95			0.047	$^3P_2 \rightarrow 3d\ ^3P_2$
3	144.63(21)		143.35	0.136(39)		0.136	$^3P_0 \rightarrow 3d\ ^3D_1$
			143.78			0.152	$^3P_2 \rightarrow 3d\ ^3D_3$
4	148.18 (4)	148.14 (4)	146.33	0.563(17)	0.563(11)	0.071	$^3P_0 \rightarrow 3d\ ^3S_1$
			146.94			0.092	$^3P_2 \rightarrow 3d\ ^3S_1$
			147.03			0.279	$^3P_0 \rightarrow 3d\ ^3P_1$
			147.27			0.330	$^3P_0 \rightarrow 3d\ ^3D_1$
			147.55			0.209	$^3P_2 \rightarrow 3d\ ^3P_2$
			147.64			0.063	$^3P_2 \rightarrow 3s\ ^3P_1$
			147.74			0.219	$^3P_2 \rightarrow 3s\ ^3D_3$
5	154.54 (9)	154.59(12)	154.99	0.083(14)	0.074(10)	0.090	$^3P_0 \rightarrow 3d\ ^3D_1$
			155.57			0.073	$^3P_2 \rightarrow 3d\ ^3D_3$
6	162.64 (9)	162.71 (7)	161.75	0.282(22)	0.224(12)	0.021	$^3P_2 \rightarrow 4d\ ^3F_3$
			161.76			0.199	$^3P_0 \rightarrow 4d\ ^3D_1$
			161.89			0.021	$^3P_2 \rightarrow 4d\ ^3F_2$
			162.11			0.036	$^3P_2 \rightarrow 4d\ ^3D_2$
			162.18			0.082	$^3P_2 \rightarrow 4d\ ^3D_3$
			162.27			0.021	$^3P_0 \rightarrow 4d\ ^3D_1$
			162.84			0.066	$^3P_2 \rightarrow 4d\ ^3D_3$
163.14	0.016	$^3P_0 \rightarrow 4d\ ^1P_1$					

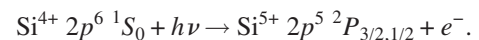
^aThe numbers refer to Fig. 2.

^bThe number in parenthesis gives the uncertainty on the last figure.

in the synthetic spectrum (second panel in Fig. 2) which includes both ground-state and excited-state photoionization and the bottom two panels of Fig. 2 where the unconvoluted calculations are shown for the discrete resonances arising from the excited state. The broad structures in the experimental data map fairly well onto groupings of resonances in the MCDF results. In view of the statistical error bars in the experimental data (Fig. 1) and the density of lines in these regions arising from the MCDF calculations we do not estimate their oscillator strengths but a detailed listing of the MCDF calculated lines is provided in Table II.

The observations for the above threshold region are of particular interest. In Fig. 3 we show an expanded view of the super-ACO data in the region of the photoionization limit, together with the results of various theoretical calculations identified in the figure caption. All the theoretical calculations [15,18,19,21,30] give results agreeing closely for

the magnitude of the above threshold cross section, arising from the description of the direct photoionization process,



This agreement between the different approaches, and with the experimental data within their uncertainties, is evidence of the weak role of electron correlation effects for this process in the energy range considered here.

The various theoretical results were obtained for Si^{4+} ions in the ground state only. In the R -matrix calculations of Ref. [5], the cross sections for ions in the $2p^5 3s\ ^3P_{0,2}$ levels were also calculated but, as they do not include the inner subshell $2p$ excitations, they are not shown on Fig. 3. The R -matrix results were convoluted with a Gaussian width of 1 eV in order to simulate the super-ACO experimental conditions.

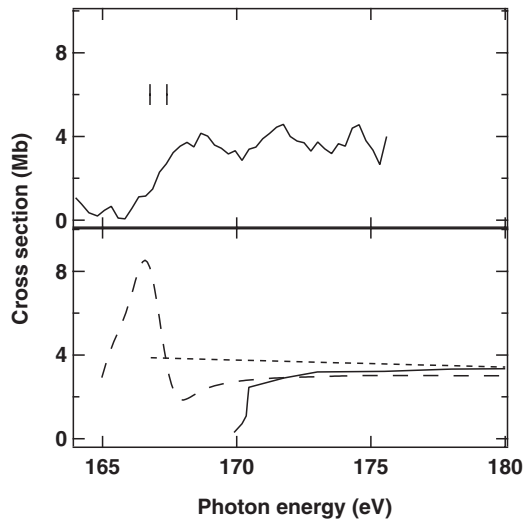


FIG. 3. Comparison of the super-ACO experimental spectrum (top panel), for the photoionization threshold region, with the results of various theoretical calculations (bottom panel): R -matrix calculations from Ref. [19] (long-dashed line); Hartree-Dirac-Slater results from Ref. [30] (short-dashed line) and RRPA calculations (solid line) from Ref. [5].

The main differences between the various theoretical calculations relate to the predicted positions of the ionization thresholds, calculated by the R matrix of Ref. [15] and the MCDF code (current work) to be lower by 1.5 eV than the tabulated values (166.77 and 167.40 eV for the ${}^2P_{3/2}$ and ${}^2P_{1/2}$ thresholds [3]). The most recent relativistic R -matrix calculations give thresholds too low by more than 3.3 eV [21] while the calculated value from the RRPA results is about 169.8 eV (see Fig. 2 of Ref. [5]). We have measured a position for the unresolved thresholds of 167.2(3) and 166.8(2) eV at super-ACO and ASTRID, respectively, in agreement with the tabulated values within experimental error.

The importance of accurately calculating the positioning of inner-shell resonances with respect to the onset of the outer-shell photoionization limit was stressed in Sec. I, as the relative energy positioning determines the calculated near-threshold cross-section behavior. Figure 3 illustrates the theoretical challenge in the context of the Si^{4+} inner-shell $2s\ {}^1S_0 \rightarrow 3p\ {}^1P_1$ resonance. The different calculations predict the position of the inner-shell transition, alternatively below [5,21] or above the ionization thresholds [15]. It is this transition which is responsible for the strong line occurring at 167 eV in the R -matrix calculated data of Fig. 3. Whereas the $2s\ {}^1S_0 \rightarrow 3p\ {}^1P_1$ resonance is clearly evident in the DLP ex-

periments of Ref. [5], because it lies below the Si^{4+} photoionization threshold it cannot give rise to a signal in the photoion experiment, unless the energy width of the resonance is sufficiently broad to overlap the limit.

The MCDF calculation for the $2s\ {}^1S_0 \rightarrow 3p\ {}^1P_1$ resonance places it at 166.36 (with the next member of the series ($2s\ {}^1S_0 \rightarrow 4p\ {}^1P_1$) at 191.6 eV). As remarked in the introduction, the RRPA calculations predict the $2s\ {}^1S_0 \rightarrow 3p\ {}^1P_1$ resonance to be the cause of an anomalously low value of the direct photoionization cross section at threshold (see Fig. 3) through the coupling of the $2p$ and $2s$ ionization channels [5]. Unfortunately, our experimental spectra lack the spectral resolution to critically test this prediction.

V. CONCLUSION

We have measured the absolute photoionization cross section of neonlike Si^{4+} ion in the 110–180 eV photon energy range. The measurements were performed using the two independent merged-beam setups of the super-ACO and ASTRID synchrotron-radiation facilities. Signals produced in the photoionization of the $2p$ subshell of Si^{4+} ions both from the $2p^6\ {}^1S_0$ ground state and the $2p^5\ 3s\ {}^3P_{0,2}$ metastable levels were observed. The data are in good agreement with calculations and the measured position of the (unresolved) $2p$ photoionization limits at 167 eV agrees within the experimental errors with the previously determined values of 166.77 and 167.40 eV. The results confirm that the inner-shell $2s$ - $3p$ resonance lies below the outer-shell $2p$ photoionization limit but the 1 eV experimental spectral resolution prevents the detailed onset of ground-state photoionization to be determined. The photoion data also provide the first observations of several resonances arising from photoionization from the excited metastable $2p^5 3s$ state, leading to estimated oscillator strengths and a comparison with detailed MCDF results which provide assignments.

ACKNOWLEDGMENTS

We would like to acknowledge the support of the Laboratoire pour l'Utilisation du Rayonnement Electromagnétique (LURE), funded by the Centre National de la Recherche Scientifique (CNRS), of the Commissariat à l'Énergie Atomique (CEA DAM), and of the European Community—Access to Research Infrastructure action of the Improving Human Potential Programme. We are grateful to the staffs of the LURE at the University of Orsay and of the Institute for Storage Ring Facilities (ISA) at the University of Aarhus for their assistance throughout the duration of the project.

- [1] M. J. Seaton, *J. Phys. B* **20**, 6431 (1987).
 [2] S. N. Nahar and A. K. Pradhan, *Phys. Rev. A* **49**, 1816 (1994).
 [3] Yu Ralchenko, A. E. Kramida, J. Reader, and *NIST ASD Team*, *NIST Atomic Spectra Database* (version 3.1.4), [Online]. Available: <http://physics.nist.gov/asd3>. National Institute of

Standards and Technology, Gaithersburg, MD, 2008.

- [4] J. P. Mosnier, M. H. Sayyad, E. T. Kennedy, J. M. Bizau, D. Cubaynes, F. J. Wuilleumier, J. P. Champeaux, C. Blancard, R. H. Varma, T. Banerjee, P. C. Deshmukh, and S. T. Manson, *Phys. Rev. A* **68**, 052712 (2003).

- [5] H. S. Chakraborty, A. Gray, J. T. Costello, P. C. Deshmukh, G. N. Haque, E. T. Kennedy, S. T. Manson, and J. P. Mosnier, *Phys. Rev. Lett.* **83**, 2151 (1999).
- [6] J. T. Costello, J.-P. Mosnier, E. T. Kennedy, P. K. Carroll, and G. O'Sullivan, *Phys. Scr.* **T34**, 77 (1991).
- [7] H. Kjeldsen, *J. Phys. B* **39**, R325 (2006).
- [8] J. B. West, *J. Phys. B* **34**, R45 (2001).
- [9] B. Kristensen, T. Andersen, F. Folkmann, H. Kjeldsen, and J. B. West, *Phys. Rev. A* **65**, 022707 (2002).
- [10] J. M. Bizau, C. Blancard, D. Cubaynes, F. Folkmann, J. P. Champeaux, J. L. Lemaire, and F. J. Wuilleumier, *Phys. Rev. A* **73**, 022718 (2006).
- [11] M. Meyer, D. Cubaynes, P. O'Keeffe, H. Luna, P. Yeates, E. T. Kennedy, J. T. Costello, P. Orr, R. Taiieb, A. Maquet, S. Dusterer, P. Radcliffe, H. Redlin, A. Azima, E. Plonjes, and J. Feldhaus, *Phys. Rev. A* **74**, 011401(R) (2006).
- [12] A. A. Sorokin, S. V. Bobashev, K. Tiedtke, and M. Richter, *J. Phys. B* **39**, L299 (2006).
- [13] C. Bostedt, H. Thomas, M. Hoener, E. Eremina, T. Fennel, K. H. Meiwes-Broer, H. Wabnitz, M. Kuhlmann, E. Plönjes, K. Tiedtke, R. Treusch, J. Feldhaus, A. R. B. de Castro, and T. Moller, *Phys. Rev. Lett.* **100**, 133401 (2008).
- [14] S. O. Kastner, K. Omidvar, and J. H. Underwood, *Astrophys. J.* **148**, 269 (1967).
- [15] A. Msezane, R. F. Reilman, S. T. Manson, and J. R. Swanson, and L. Armstrong, Jr, *Phys. Rev. A* **15**, 668 (1977).
- [16] P. Shorer, *Phys. Rev. A* **20**, 642 (1979).
- [17] T. N. Chang and T. Olsen, *Phys. Rev. A* **24**, 1091 (1981).
- [18] M. Lamoureux and V. Radojević, *J. Phys. B* **15**, 1341 (1982).
- [19] A. Hibbert and M. P. Scott, *J. Phys. B* **27**, 1315 (1994).
- [20] A. Hibbert, M. LeDourneuf, and M. Mohan, *At. Data Nucl. Data Tables* **53**, 23 (1993).
- [21] A. K. S. Jha, N. Singh, N. Verma, and M. Mohan, *Can. J. Phys.* **84**, 707 (2006).
- [22] H. S. Chakraborty, P. C. Deshmukh, E. W. B. Dias, and S. T. Manson, *Astrophys. J.* **537**, 1094 (2000).
- [23] J.-M. Bizau, E. Bouisset, C. Blancard, J.-P. Champeaux, A. Compant La Fontaine, C. Couillaud, D. Cubaynes, D. Hitz, C. Vinsot, and F. W. Wuilleumier, *Nucl. Instrum. Methods Phys. Res. B* **205**, 290 (2003).
- [24] H. Kjeldsen, F. Folkmann, J. van Elp, H. Knudsen, J. B. West, and T. Andersen, *Nucl. Instrum. Methods Phys. Res. B* **234**, 349 (2005).
- [25] R. N. S. Sodhi and C. E. Brion, *J. Electron Spectrosc. Relat. Phenom.* **34**, 363 (1984).
- [26] G. Tachiev and C. Froese Fischer (2002); Available: <http://atoms.vuse.vanderbilt.edu/>
- [27] J.-M. Bizau, J.-P. Champeaux, D. Cubaynes, F. J. Wuilleumier, F. Folkmann, T. S. Jacobsen, F. Penent, C. Blancard, and H. Kjeldsen, *Astron. Astrophys.* **439**, 387 (2005).
- [28] J. Bruneau, *J. Phys. B* **17**, 3009 (1984).
- [29] U. Fano and J. W. Cooper, *Rev. Mod. Phys.* **40**, 441 (1968).
- [30] D. A. Verner and D. G. Yakovlev, *Astron. Astrophys. Suppl. Ser.* **109**, 125 (1995).